Biosensors and Bioelectronics 83 (2016) 281–286

Contents lists available at ScienceDirect

Biosensors and Bioelectronics

journal homepage: www.elsevier.com/locate/bios

Initiator-catalyzed self-assembly of duplex-looped DNA hairpin motif based on strand displacement reaction for logic operations and amplified biosensing

Sai Bi [a,*], Shuzhen Yue [a], Qiang Wu [b], Jiayan Ye [c]

[a] Collaborative Innovation Center for Marine Biomass Fiber Materials and Textiles, College of Chemistry and Chemical Engineering, Laboratory of Fiber Materials and Modern Textiles, the Growing Base for State Key Laboratory, Shandong Sino-Japanese Center for Collaborative Research of Carbon Nanomaterials, Qingdao University, Qingdao 266071, PR China

[b] Key Laboratory for Sustainable Development of Marine Fisheries, Ministry of Agriculture, Shandong Provincial Key Laboratory for Fishery Resources and Eco-environment, Yellow Sea Fisheries Research Institute, Chinese Academy of Fishery Sciences, Qingdao 266071, PR China

[c] Key Laboratory of Sensor Analysis of Tumor Marker, Ministry of Education, College of Chemistry and Molecular Engineering, Qingdao University of Science and Technology, Qingdao 266042, PR China

ARTICLE INFO

Article history:
Received 18 March 2016
Received in revised form
16 April 2016
Accepted 19 April 2016
Available online 20 April 2016

Keywords:
Biosensor
Catalytic self-assembly
Keypad lock
Logic gates
Strand displacement

ABSTRACT

Here we program an initiator-catalyzed self-assembly of duplex-looped DNA hairpin motif based on strand displacement reaction. Due to the recycling of initiator and performance in a cascade manner, this system is versatilely extended to logic operations, including the construction of concatenated logic circuits with a feedback function and a biocomputing keypad-lock security system. Compared with previously reported molecular security systems, the prominent feature of our keypad lock is that it can be spontaneously reset and recycled with no need of any external stimulus and human intervention. Moreover, through integrating with an isothermal amplification technique of rolling circle amplification (RCA), this programming catalytic DNA self-assembly strategy readily achieves sensitive and selective biosensing of initiator. Importantly, a magnetic graphene oxide (MGO) is introduced to remarkably reduced background, which plays an important role in enhancing the signal-to-noise ratio and improving the detection sensitivity. Therefore, the proposed sophisticated DNA strand displacement-based methodology with engineering dynamic functions may find broad applications in the construction of programming DNA nanostructures, amplification biosensing platform, and large-scale DNA circuits.

1. Introduction

Nucleic acids have emerged as versatile materials due to their unique features of sequence programmability, controllable synthesis and high stability, which allow rational design of complex molecular architectures that are assembled and engineered from defined sequences with high accuracy and precision (Y.-J. Chen et al., 2015; Pinheiro et al., 2011). In dynamic DNA nanotechnology, besides DNA enzyme-activated systems (Gerasimova et al., 2014; Kong et al., 2013; Feng et al., 2012), strand displacement reaction has demonstrated its powerful capability to build molecular dynamic systems (Yu and Seeling, 2011). A typical strand displacement reaction is usually initiated by a short single-stranded overhang region (denoted as a toehold), in which the toehold facilitates the branch migration to displace the resident strand from a double-stranded complex (Machinek et al., 2014; Zhang and Winfree, 2009). Up to now, strand displacement reactions have been ingeniously implemented in assembly of DNA nanostructures (Dirks and Pierce, 2004; Kim et al., 2015; Zhang et al., 2013) and construction of diverse molecular machines (Song and Liang, et al., 2012; Li et al., 2015; Xu et al., 2015). Moreover, the emergence of this methodology has enabled the construction of programming catalytic systems (Zhang et al., 2007; Yao et al., 2015), digital logic circuits (Qian and Winfree, 2011; Bi et al., 2015b), and cascade reaction networks (Han et al., 2015; Liu et al., 2015), which have been widely applied in the fields of biomedicine, biotechnology, and nanoeletronics.

Catalytic hairpin assembly (CHA) is one of the most notable examples of toehold-mediated strand displacement reaction to control the programming assembly and disassembly of DNA hairpins catalyzed by a DNA input (Yin et al., 2008). On the basis of CHA, a variety of dynamic functions have been achieved, which is represented by the catalytic formation of mulitbranched junctions,

* Corresponding author.
E-mail address: bisai11@126.com (S. Bi).

http://dx.doi.org/10.1016/j.bios.2016.04.059
0956-5663/

the construction of complex catalytic circuits, and autonomous locomotion of DNA walkers (Wang et al., 2014). Since the principle of CHA was put forward, great efforts have been made to improve its performance and extend its applications (Li et al., 2011; Jiang et al., 2014). Because hundreds-fold catalytic amplification reactions can be occurred during a CHA process, CHA has been integrated with various isothermal amplification techniques, such as rolling circle amplification (RCA) (Jiang et al., 2013; Zhuang et al., 2014), hybridization chain reaction (HCR) (Li et al., 2012; Jiang et al., 2012; Wei et al., 2016; Feng et al., 2015), and enzyme-catalyzed amplification systems (Tao et al., 2015; Song et al., 2015), to develop as dramatic signal amplification platforms for sensitive detection of various biomolecules (Jung and Ellington, 2014). While extensive studies have been carried out to investigate CHA, it is still a challenge to develop this principle with new reaction pathways to form DNA assembly in novel patterns.

Moreover, a variety of DNA strand displacement-based logic gates (Janssen et al., 2015), circuits (Groves et al., 2015; Zhang et al., 2016), and even neural networks (Qian et al., 2011) have been developed for complicated computations with high efficiency and accuracy. For practical applications, many issues can be abstracted into logic relationships and solved by the corresponding logic operations (Xie et al., 2011; Chen et al., 2013; Rudchenko et al., 2013; Amir et al., 2014). In particular, as a smart logic device, the keypad lock has drawn increasing attention since the open of a keypad lock is dependent on not only the proper combination of inputs but also the correct order (Y.-J. Chen et al., 2015; J. Chen et al., 2015). Thus, keypad lock provides a new approach for protecting information to defend illegal invasion at the molecular level. To meet the growing needs of designing complex molecular logic circuits, it is desirable to develop a keypad-lock security system with more complicated functions.

Herein, a programming catalytic DNA self-assembly strategy is proposed, which consists of one circular strand (C), two hairpins (H1 and H2), and one initiator (I). In this system, strand I activates a cascade of assembly steps with C, H1 and H2, followed by a disassembly step in which I is displaced by H2 from the complex, resulting in the formation of duplex-looped DNA hairpin motif and re-release of I for multiple turnover. Since the assembly process is performed in the cascade manner, this principle is successfully exploited to construct concatenated logic circuits with a feedback function by anchoring initiator on magnetic nanoparticles (MNPs), which then operates as a keypad lock at the molecular level that can be automatically reset to the initial state without an external stimulus. Moreover, this system is readily and rationally combines with the isothermal amplification technique of RCA using magnetic graphene oxide (MGO) to significantly reduce background and enhance the signal-to-noise ratio, achieving amplified biosensing platform for highly sensitive and selective detection of DNA.

2. Experimental section

2.1. Preparation of circular strand C

Circular strand C was prepared by self-templated ligation of 5′-phosphorylated dumbbell-shaped DNA sequences by T4 DNA ligase (the schematic DNA constructer of C is shown in Fig. S1). Briefly, strand C (0.1 mM) was firstly annealed by heating at 90 °C for 5 min and cooling down to 25 °C at a rate of 0.1 °C/s. The resultant solution was allowed to stand at 25 °C for 2 h at least to obtain the dumbbell structure. Then, the ligation reaction was carried out by mixing 5 μL of annealed C (0.1 mM), 5 μL of 10 × T4 DNA ligase buffer (400 mM Tris–HCl, 100 mM $MgCl_2$, 100 mM DTT, 5 mM ATP, pH 7.8), 1 μL of T4 DNA ligase (5 U). The total volume of the solution was supplemented to 50 μL by ultrapure nuclease-free water, followed by incubation at 22 °C for 2 h. The reaction was terminated by heating at 65 °C for 10 min to inactivate T4 DNA ligase. The resultant circular strand C was cooled down to room temperature (~25 °C) for 1 h and stored at −20 °C before use.

2.2. Preparation of magnetic graphene oxide (MGO)

The MGO was prepared according to the previously reported methods (Bi et al., 2015a). Briefly, 10 mg graphene oxide (GO) was dispersed in 10 mL of water. After ultrasonicated for 30 min, 600 μL of the GO solution was mixed with 600 μL of EDC (0.1 M) and 300 μL of NHS (0.1) in imidazole-HCl buffer (0.1 M, pH 6.8), followed by reaction at 37 °C for 1 h to activate carboxyl groups on GO. Then, 300 μL of amino-coated magnetic microparticles (MMPs) (10 mg/mL) was added and incubated at 37 °C overnight. The resulting MMP-GO conjugates, termed as magnetic graphene oxide (MGO), was washed three times with PBS (0.01 M, pH 7.4) and re-dispersed in the same buffer for further use.

2.3. Real-time fluorescence measurements

A typical real time fluorescent measurement for a self-assembly process involving circular C, 4-(4-dimethylaminophenylazo)benzoyl (Dabcyl)-modified H1, fluorescein isothiocyanate (FITC)-modified H2, and initiator is as follows. Firstly, to make sure the desirable secondary structures of C, H1, and H2, the strands with the concentration of 1 × (10 μM) were respectively annealed in TE buffer (10 mM Tris–HCl, 1 mM EDTA-2Na) supplemented with 12.5 mM $MgCl_2$ (pH 8.0) before use (heat at 90 °C for 5 min, cool to 25 °C at a rate of 0.1 °C/s, and stand at 25 °C for 2 h at least). Then, 2 μL of each annealed specie of C, H1 and H2 (1 × for each) and 32 μL of TE buffer were mixed. Upon introducing of 2 μL of I with different concentrations, the fluorescence readings over time were monitored immediately on a LineGene 9600 Real-Time fluorescence detection system (Hangzhou, China) at an interval of 30 s (λ_{ex}=470 nm and λ_{em}=525 nm). The reaction temperature was set as 37 °C.

2.4. Operation of the concatenated logic circuits

The initial state of the concatenated logic circuits was 2 μL of 1 × (10 μM) strand I and 32 μL of TE buffer. Upon the introduction of inputs A, B and C (2 μL for each) with different combinations of (0,0,0), (0,0,1), (0,1,0), (0,1,1), (1,0,0), (1,0,1), (1,1,0) and (1,1,1) into the system, the fluorescence readings over time were monitored immediately on a LineGene 9600 Real-Time fluorescence detection system (Hangzhou, China) at an interval of 30 s (λ_{ex}=470 nm and λ_{em}=525 nm). The reaction temperature was set as 37 °C. The input "0" was substituted by corresponding volume of TE buffer.

2.5. Execution of keypad lock

Firstly, strand I was immobilized on MNPs according to the previously reported work (Bi et al., 2014). For the operation of inputs (ABC), the strand I-anchored MNPs solution was incubated with input A (1 ×, 10 μM) for 30 min. After washing the resulting MNPs with PBS buffer three times, input B (1 ×, 10 μM) was added and incubated for 30 min, followed by a magnetic washing procedure. Then, the MNP complexes were further reacted with input C (1 ×, 10 μM) for 30 min. After magnetic separation, the supernatant was collected for fluorescence detection on a LineGene 9600 Real-Time fluorescence detection system (Hangzhou, China) at an interval of 30 s (λ_{ex}=470 nm and λ_{em}=525 nm). The operation of other input permutations (ACB, BAC, BCA, CAB, and CBA) was performed in the same way as mentioned above.

2.6. RCA reaction and measurements

Firstly, the assembly reactions were triggered by mixing C, H1, and H2 (2 μL for each with a concentration of 0.01 × (0.1 μM)) with 2 μL of varied concentrations of I and carried out by incubating at 37 °C for 1 h. Then, 100 μL of the as-prepared MGO was added, followed by incubation at room temperature for 10 min. After magnetic separation, the RCA reaction was performed in a volume of 20 μL made from 1 μL of Klenow (exo-) DNA polymerase (5 U), 2 μL of 10 × Klenow (exo-) DNA polymerase buffer (500 mM Tris–HCl, 50 mM $MgCl_2$, and 10 mM DDT, pH 8.0), 9 μL of dNTPs (10 mM), and 8 μL of the above resulting supernatant products. After incubation at 37 °C for 2 h, the RCA reaction was terminated by heating at 90 °C for 10 min to inactivate the polymerase. The RCA products were mixed with 1 μL of SYBR Green I (20 ×) at 37 °C for 30 min. The fluorescence intensity was recorded on a LineGene 9600 Real-Time fluorescence detection system (Hangzhou, China) at an interval of 30 s (λ_{ex}=470 nm and λ_{em}=525 nm). The reaction temperature was set as 37 °C.

3. Results and discussion

3.1. Principle of the catalytic self-assembly pathways

Herein, we propose a programming catalytic strategy for self-assembly of duplex-looped DNA hairpin motifs. The system consists of one circular strand (C), two hairpins (H1 and H2), and one initiator (I) (Scheme 1(a)). The assembly and disassembly pathways are specified in Scheme 1(b). In the absence of I, C, H1, and H2 metastably coexist. Upon the introduction of I into the system, I first hybridizes to the loop domain a of C to form the complex I · C, resulting in partially opening the stem of C. Then, the domain b* of H1 binds the newly exposed segment b of C, which further initiates toehold-mediated strand displacement reaction that completely opens C and H1 and produces the I · C · H1 hybrid. Furthermore, the newly accessible domain d of H1 binds to the single-stranded toehold d* of H2, which then rearranges by DNA branch migration to open H2. As a result, the librated loop b-c of H2 hybridizes to the single-stranded region b*-c* of C, leading to the generation of the I · C · H1 · H2 intermediate. Due to the inherently instability of this intermediate, a spontaneous dissociation occurs in which H2 displaces I from the complex, resulting in the formation of a duplex-looped DNA hairpin as product (Scheme 1(c)) and regeneration of I to catalyze additional self-assembly processes.

It should be noted that to avoid false hybridization of single-stranded overhang b*-c* of H1 with loop domain b-c of H2, two base pairs are manually designed in the loop of H1 (the predicted schematic constructers of the DNA species are shown in Fig. S1 in the Supporting Information). In addition, although the sequence of domain a of C is complementary to domain a* of H1, the two domains are in loops with only 14 nucleotides in length, which thus prevents their hybridization. The catalytic reaction pathways are confirmed by non-denaturing polyacrylamide gel electrophoresis (PAGE) (see Supporting Information, Section S2).

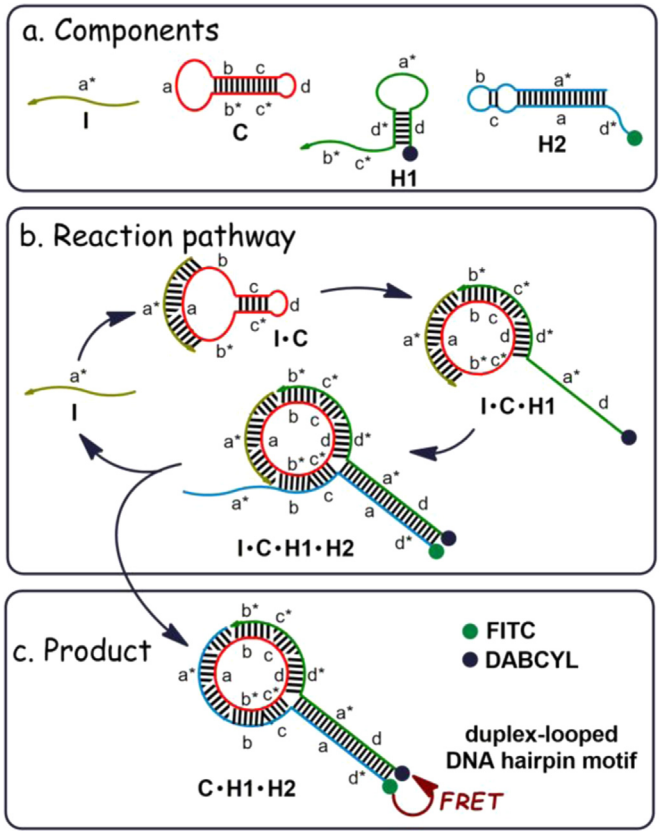

Scheme 1. Programming catalytic self-assembly of duplex-looped DNA hairpin motif. (a) Components of the system. Letter labels denote functional domains. Domain x* represents the complementary domain of x. (b) Specific reaction pathways of the proposed strategy, and (c) the resultant product in the structure of duplex-looped DNA hairpin.

3.2. System kinetics

To investigate the kinetics of the above system quantitatively, quencher Dabcyl and fluorophore FITC are labeled at 5′ terminus of H1 and 3′ terminus of H2, respectively (Scheme 1), to perform the fluorescence quenching experiments. As shown in Fig. 1, concentrations of I in a 10^4-fold range (from 0.0001 × to 1 ×) are introduced into the system containing C, H1, and H2 to initiate the assembly process. The time-dependent fluorescence intensity of FITC is measured (λ_{ex}=470 nm and λ_{em}=525 nm) every 30 s for 180 min. At the beginning of the reaction, all of the fluorescence intensities are high since the reactants are initially free in solution, making the fluorophore labeled on H2 far away from the quencher on H1. Moreover, I initiates the formation of duplex-looped DNA hairpin in a closed structure, which brings the fluorophore and the

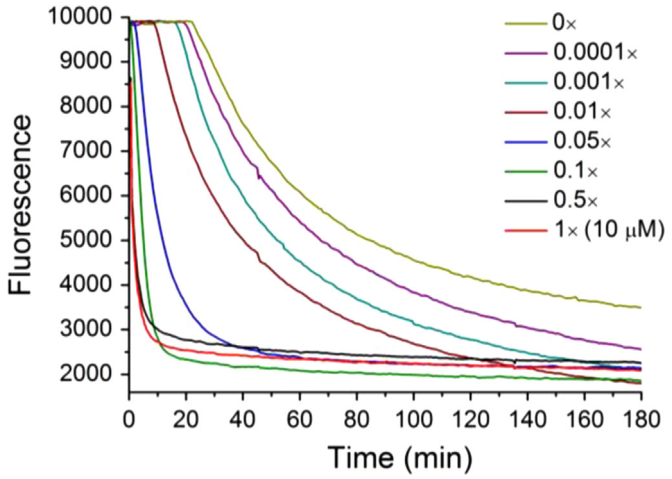

Fig. 1. System kinetics by treating the system consisted of C, H1 and H2 with different amounts of I and monitoring real-time fluorescence. The concentration of each species (C, H1 and H2) initially added is 10 μM (1 ×). The plot labels on the right-hand side represent the number of equivalents of I added into the reaction system. Note: the concentration of I for 0.0001 × corresponds to a concentration of 1 nM.

quencher into a close proximity spatially and results in the decrease in fluorescence signal. Substoichiometric quantities of I (1×, 0.5×, 0.1×, 0.05×) enable the fluorescence to decrease dramatically and rapidly reach almost the same plateau due to the depletion of reactants. When the concentration of each species is 1× (10 μM), the reaction approaches completion within 10 min. The fastest reaction rate is occurred within 2 min, which shows a linear kinetics. Thus, the V_{max} and k_{cat} are estimated to be 3.37×10^{-6} M/min and 0.34 min^{-1}, respectively. Spontaneous initiation in the absence of I (0×) reflects the system leakage. Thus, to improve the purity and stability of species in perfect secondary structures plays an important role in decreasing system leakage (Yin et al., 2008). Although the system leakage is inevitable due to the unpurified strand and denature, given the sensitivity of the fluorometer, the melting temperature of DNA reactants and the reaction rate, the reaction conditions have been optimized as the initial concentrations of H1, H2 and C are 1× (10 μM) and the reaction temperature is 37 °C. Fortunately, although there is a leakage of the system, its kinetics is slower than the initiator triggered one, which can be clearly distinguished from 0.0001× I. In addition, this catalytic self-assembly system also exhibits excellent sequence specificity to distinguish the target initiator from the mismatched one, since a mismatch in either toehold or branch migration regions should impede toehold-mediated strand displacement generally by at least one order of magnitude (see Supporting Information, Section S3) (Li et al., 2011).

3.3. Concatenated logic circuits

Given the assembly of duplex-looped DNA hairpin in a cascade manner, the proposed system can be considered as a network composed of concatenated YES-AND-AND logic gates (Fig. 2). In the concatenated circuits, C, H1 and H2 involving stepwise treatment in Scheme 1 are acted as inputs (inputs A, B and C) with quencher Dabcyl labeled at 5′ terminus of H1 and fluorophore FITC at 3′ terminus of H2. The inputs are defined as 1 when they are present, whereas as 0 if they are absent. The output is the FRET signal of the system, which is considered as 1 when the fluorescence value is between 100 and 9000, otherwise (that is, if the fluorescence value is below 100 or above 9000) as 0. For the operations, the initial state of a single-stranded I hybridizes with input A to form the hybrid I·A that acts as the output of the YES gate and the input of the downstream gate. Then, the first AND gate (AND1) is activated by I·A and input B, yielding a complex I·A·B. Ultimately, input C and the resultant complex trigger the second AND gate (AND2) to produce the duplex-looped DNA

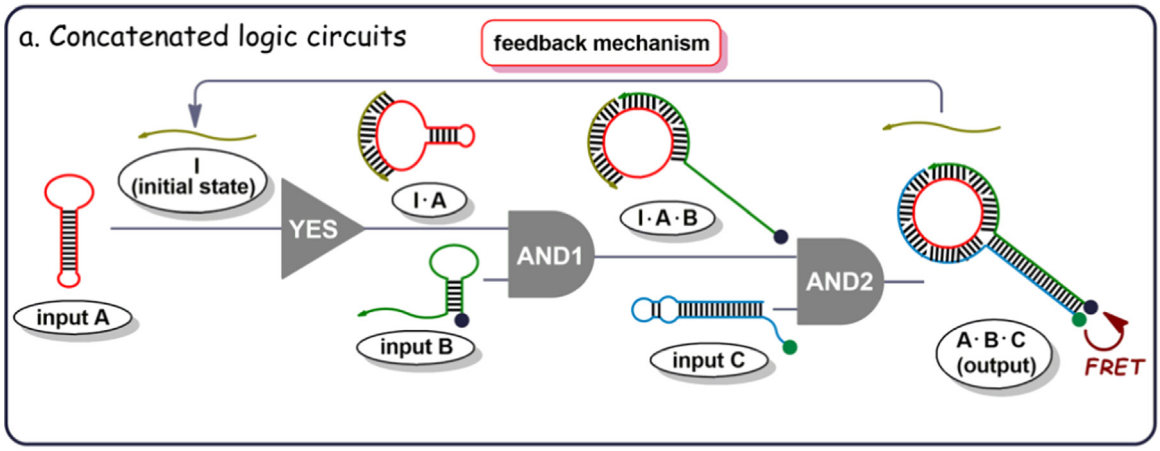

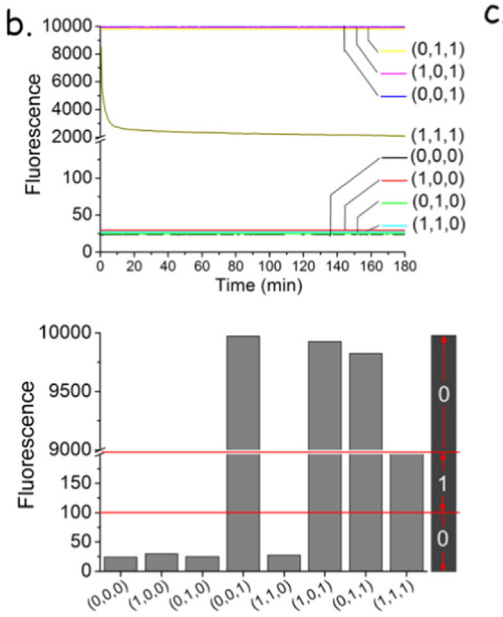

c.

Inputs			Product	Output
A	B	C		Quenched fluorescence
0	0	0	No DNA	0
1	0	0		0
0	1	0		0
0	0	1		0
1	1	0		0
1	0	1		0
0	1	1		0
1	1	1	FRET	1

Fig. 2. Three-input concatenated YES-AND-AND logic circuits based on catalytic self-assembly of duplex-looped DNA hairpin. (a) Schematic illustration, (b) fluorescence kinetic curves and corresponding fluorescence intensities after reaction for 180 min, and (c) truth table of the concatenated logic circuits. The concentrations of each input and I initially added are 10 μM (1×). The red line in (b) indicates the threshold fluorescence value.

hairpin motif A·B·C as the output. This closed structure allows the fluorophore on H2 in close proximity to the quencher on H1, which results in a decreased fluorescence signal after reaction for 180 min.

The fluorescence intensities resulting from the operation of the three-input concatenated logic circuits with different input states and corresponding truth table are presented in Fig. 2(b) and (c), respectively. Fig. 2(c) shows the products corresponding to different input combinations. Accordingly, the FRET signal with a fluorescence value of ~2000 ("1" output) is only detected when all the three inputs are present (1,1,1), whereas for other input combinations the fluorescence signal is too high (above 9000, for the inputs of (0,0,1), (1,0,1), and (0,1,1)) or too low (below 100, for the inputs of (0,0,0), (1,0,0), (0,1,0), and (1,1,0)) and reads as "0" output. Therefore, the results are consistent with the operation of a YES-AND-AND concatenated logic circuits. More importantly, since the initiator can be automatically recycled during the self-assembly of duplex-looped DNA hairpin motif, a feedback mechanism is endowed to this logic system, which can be readily applied to amplified detection of inputs, especially nucleic acid molecules (e.g. DNA, microRNA, and mRNA), through tailoring of an appropriate substrate for amplification of the gate output. In addition, molecular computing holds great promise for controlling biological progresses, such as gene regulation and disease diagnosis at the molecular level.

Moreover, a molecular keypad lock security system can be constructed based on the proposed concatenated logic circuits by anchoring strand I on magnetic nanoparticles (MNPs) (see Supporting Information, Section S4).

3.4. RCA biosensing platform

In the catalytically formed duplex-looped DNA hairpin structure, a circular strand C is a central component to support the duplex-looped domain. Ingeniously, the concept of rolling circle amplification (RCA) is introduced for isothermal amplified biosensing, which is initiated in the presence of DNA polymerase/dNTPs using the dumbbell-shaped circular strand C as template and H1 as primer (Fig. 3(a)). During the RCA, a long DNA sequence contains numerous dumbbell probes that are complementary to the circular template C is produced. The RCA products can be easily observed by 15% native PAGE, which is too large to enter the gel by electrophoresis (Fig. S2, lane 5). As a result, the double-stranded specific dye SYBR Green I can intercalate into the duplex region of the resulting RCA products to generate an enhanced fluorescence.

It should be noted that in the absence of I, although no duplex-looped DNA hairpin is formed and no RCA is initiated theoretically to yield a long stranded product, the stems of probes C, H1 and H2 can inherently bind with SYBR Green I, which inevitably induce a high background that affects the detection sensitivity. In view of this problem, a magnetic graphene oxide (MGO) is introduced into the system. In this study, the MGO conjugates are readily prepared via covalently linking amino groups on magnetic nanoparticles (MNPs) to carboxyls on GO, which are characterized by SEM (Fig. 3(d)). Owing to the high binding affinity of GO for single-stranded DNA through strong π-π stacking interactions (Bi et al., 2012), the unreacted DNA probes can be effectively absorbed on GO surface and easily removed through magnetic separation, leading to a low background fluorescence. On the other hand, initiator induced DNA assembly are in completely duplex structure, which resists the absorption by MGO. The significantly reduced background plays an important role in enhancing the signal-to-noise ratio and improving the detection sensitivity. After optimization of the RCA reaction conditions (see Supporting Information, Section S5), a series of I with different concentrations are detected using the proposed biosensing platform. From Fig. 3(b), a weak fluorescence signal is observed in the absence of strand I (0 ×). Significantly,

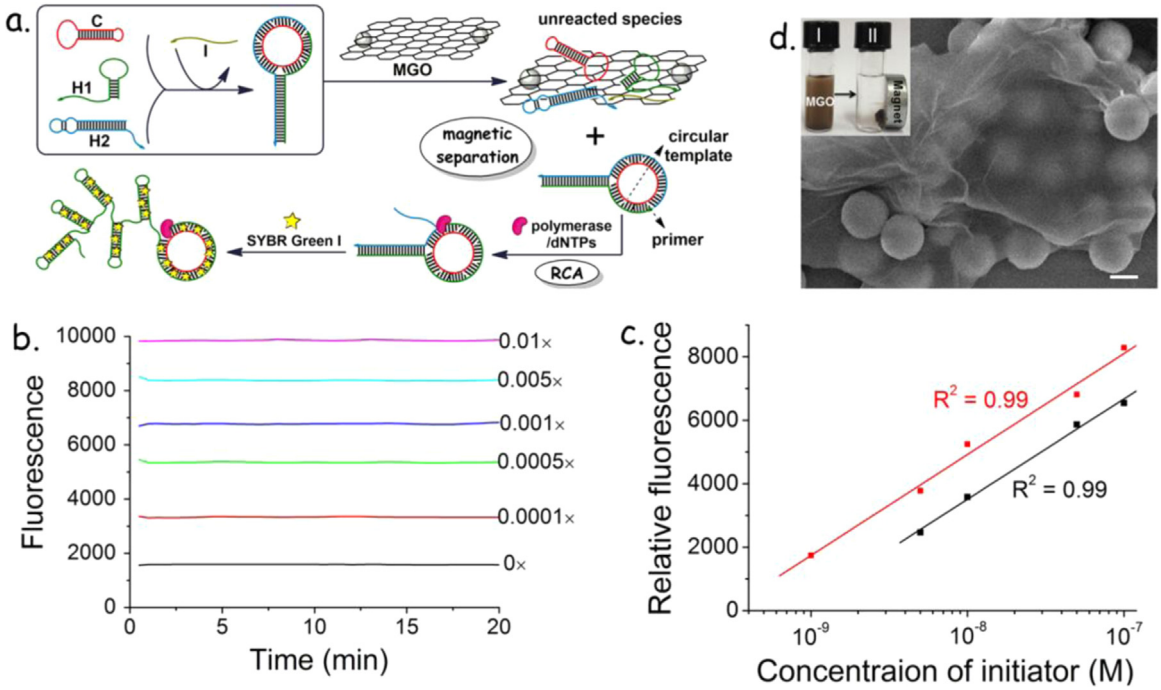

Fig. 3. Catalytic self-assembly of duplex-looped DNA hairpin-based RCA for amplified biosensing. (a) Schematic illustration of RCA using MGO to magnetically remove unreacted DNA species through π-stacking interactions to reduce background. (b) Fluorescence kinetic curves after RCA, and (c) calibration curves obtained by using MGO (red curve) and without MGO (black curve). The relative fluorescence is calculated by F-F0, where F0 and F are the fluorescence intensities without and with initiator, respectively. The concentration of each species (C, H1 and H2) initially added is 0.1 μM (0.01 ×). The plot labels on the right-hand side of (b) represent the number of equivalents of I added into the reaction system. (d) SEM image of the prepared MGO conjugates (scale bar: 1 μm). Inset: Photographs of the MGO before (I) and after (II) magnetic separation.

0.0001 × I can be reliably distinguished with 0 × I after catalytic self-assembly of duplex-looped DNA hairpin motif within 1 h and RCA reaction for 2 h. Moreover, the fluorescence intensities increase with increasing the concentrations of I. From the red curve of Fig. 3(c), a linear relationship is obtained between I concentration in logarithmic scale and relative fluorescence intensity when the concentrations of I are in the range from 0.0001 × (corresponding to a concentration of 10^{-9} M) to 0.01 × (corresponding to a concentration of 10^{-7} M) with a determination coefficient (R^2) of 0.99 (n=5). The limit of detection (LOD) is estimated to be 8.4 × 10^{-10} M (3σ), which is 5-fold lower than that obtained without the use of MGO (black curve of Fig. 3(c). Certainly, this high sensitivity can be attributed to not only the amplification effect of RCA and employment of MGO to reduce background noise, but also the recycling of I in the process to assemble duplex-looped DNA hairpin motif. In addition, the relative standard deviation (RSD) is estimated to be 6.1% from five repeated measurements of 0.0005 × I, demonstrating a good reproducibility and stability of this method.

Moreover, to verify the selectivity of the proposed biosensing system, control experiments are carried out by incubating H1, C and H2 with mutant initiator at different concentrations. From Fig. S6, even the concentration as high as 0.01 ×, the fluorescence signals generated by mutants are very small that are comparable to that of the blank, while the complementary initiator produces an obvious change in fluorescence signal. Thus, the proposed assay demonstrates an excellent selectivity for DNA detection.

4. Conclusion

In summary, the present study has introduced a programming pathway for catalytic self-assembly of duplex-looped DNA hairpin motif based on toehold-mediated strand displacement. Since the initiator can be recycled automatically and the assembly process are performed in a cascade manner, this system is successfully applied to construct concatenated logic circuits with a feedback function and is further developed as a biocomputing keypad-lock security system. In comparison with traditional molecular keypad locks, our keypad lock can be readily reset without the requirement of any external stimulus and human intervention. Moreover, through integrating with isothermal amplification technique of RCA, this strategy has readily achieved highly sensitive biosensing of initiator using MGO to reduce background and improve the detection sensitivity. Indeed, the present assay can be extended to develop more powerful logic and biosensing platforms with enhanced complexity for the activation of cascaded circuits by different biocatalysts, which represents exciting future opportunities in DNA nanotechnology, such as biomedicine, nanosensors, DNA computation, and nanodevices.

Acknowledgement

This work was supported by the National Natural Science Foundation of China (21375056 and 21535002), the Program for New Century Excellent Talents in University of Ministry of Education of China (NCET-12–1024), the Natural Science Foundation of Qingdao (15–9-1–107-jch), and the Open Funds of the Shandong Province Key Laboratory of Detection Technology for Tumor Markers (KLDTTM2015–1).

Appendix A. Supporting information

Supplementary data associated with this article can be found in the online version at doi:10.1016/j.bios.2016.04.059.

References

Amir, Y., Ben-Ishay, E., Levner, D., Ittah, S., Abu-Horowitz, A., Bachelet, I., 2014. Nat. Nanotechnol. 9, 353–357.
Bi, S., Chen, M., Jia, X., Dong, Y., 2015a. Nanoscale 7, 3745–3753.
Bi, S., Cui, Y., Dong, Y., Zhang, N., 2014. Biosens. Bioelectron. 53, 207–213.
Bi, S., Ye, J., Dong, Y., Li, H., Cao, W., 2015b. Chem. Commun. 52, 402–405.
Bi, S., Zhao, T., Luo, B., 2012. Chem. Commun. 48, 106–108.
Chen, J., Zhou, S., Wen, J., 2015. Angew. Chem. Int. Ed. 54, 446–450.
Chen, Y.-J., Dalchau, N., Srinivas, N., Phillips, A., Cardelli, L., Soloveichik, D., Seelig, G., 2013. Nat. Nanotechnol. 8, 755–762.
Chen, Y.-J., Groves, B., Muscat, R.A., Seeling, G., 2015. Nat. Nanotechnol. 10, 748–760.
Dirks, R.M., Pierce, N.A., 2004. Proc. Natl. Acad. Sci. USA 101, 15275–15278.
Feng, C., Zhu, J., Sun, J., Jiang, W., Wang, L., 2015. Talanta 143, 101–106.
Feng, K., Kong, R., Wang, H., Zhang, S., Qu, F., 2012. Biosens. Bioelectron. 38, 121–125.
Gerasimova, Y.V., Kolpashchikov, D.M., 2014. Chem. Soc. Rev. 43, 6405–6438.
Groves, B., Chen, Y.-J., Zuria, C., Pochekailov, S., Kirschman, J.L., Santangelo, P.J., Seelig, G., 2015. Nat. Nanotechnol. 11, 287–294.
Han, D., Wu, C., You, M., Zhang, T., Wan, S., Chen, T., Qiu, L., Zheng, Z., Liang, H., Tan, W., 2015. Nat. Chem. 7, 835–841.
Janssen, B.M.G., van Rosmalen, M., van Beek, L., Merkx, M., 2015. Angew. Chem. Int. Ed. 54, 2530–2533.
Jiang, Y.S., Bhadra, S., Li, B., Ellington, A.D., 2014. Angew. Chem. Int. Ed. 53, 1845–1848.
Jiang, Y., Li, B., Chen, X., Ellington, A.D., 2012. Molecules 17, 13211–13220.
Jiang, Y., Li, B., Milligan, J.N., Bhadra, S., Ellington, A.D., 2013. J. Am. Chem. Soc. 135, 7430–7433.
Jung, C., Ellington, A.D., 2014. Acc. Chem. Res. 47, 1825–1835.
Kim, J., Lee, J., Hamada, S., Murata, S., Park, S.H., 2015. Nat. Nanotechnol. 10, 528–533.
Kong, R.-M., Fu, T., Sun, N.-N., Qu, F.-L., Zhang, S.-F., Zhang, X.-B., 2013. Biosens. Bioelectron. 50, 351–355.
Li, B., Ellington, A.D., Chen, X., 2011. Nucleic Acids Res. 39, e110.
Li, B., Jiang, Y., Chen, X., Ellington, A.D., 2012. J. Am. Chem. Soc. 134, 13918–13921.
Li, X., Li, D., Zhou, W., Chai, Y., Yuan, R., Xiang, Y., 2015. Chem. Commun. 51, 11084–11087.
Liu, B., Chen, J., Wei, Q., Zhang, B., Zhang, L., Tang, D., 2015. Biosens. Bioelectron. 69, 241–248.
Machinek, R.R.F., Ouldridge, T.E., Haley, N.E.C., Bath, J., Turberfield, A.J., 2014. Nat. Commun. 5, 5324.
Pinheiro, A.V., Han, D., Shih, W.M., Yan, H., 2011. Nat. Nanotechnol. 6, 763–772.
Qian, L., Winfree, E., 2011. Science 332, 1196–1201.
Qian, L., Winfree, E., Bruck, J., 2011. Nature 475, 368–372.
Rudchenko, M., Taylor, S., Pallavi, P., Dechkovskaia, A., Khan, S., Butler Jr, V.P., Rudchenko, S., Stojanovic, M.N., 2013. Nat. Nanotechnol. 8, 580–586.
Song, T., Liang, H., 2012. J. Am. Chem. Soc. 134, 10803–10806.
Song, W., Zhang, Q., Sun, W., 2015. Chem. Commun. 51, 2392–2395.
Tao, C., Yan, Y., Xiang, H., Zhu, D., Cheng, W., Ju, H., Ding, S., 2015. Chem. Commun. 51, 4220–4222.
Wang, F., Lu, C.-H., Willner, I., 2014. Chem. Rev. 114, 2881–2941.
Wei, Y., Zhou, W., Li, X., Chai, Y., Yuan, R., Xiang, Y., 2016. Biosens. Bioelectron. 77, 416–420.
Xie, Z., Wroblewska, L., Prochazka, L., Weiss, R., Benenson, Y., 2011. Science 333, 1307–1311.
Xu, J., Wu, Z.-S., Shen, W., Xu, H., Li, H., Jia, L., 2015. Biosens. Bioelectron. 73, 19–25.
Yao, D., Song, T., Sun, X., Xiao, S., Huang, F., Liang, H., 2015. J. Am. Chem. Soc. 137, 14107–14113.
Yin, P., Choi, H.M.T., Calvert, C.R., Pierce, N.A., 2008. Nature 451, 318–322.
Yu, D., Seeling, G., 2011. Nat. Chem. 3, 103–113.
Zhang, D.Y., Hariadi, R.F., Choi, H.M.T., Winfree, E., 2013. Nat. Commun. 4, 1965.
Zhang, D.Y., Turberfield, A.J., Yurke, B., Winfree, E., 2007. Science 318, 1121–1125.
Zhang, D.Y., Winfree, E., 2009. J. Am. Chem. Soc. 131, 17303–17314.
Zhang, Z., Li, J.L., Yao, J., Wang, T., Yin, D., Xiang, Y., Chen, Z., Xie, G., 2016. Biosens. Bioelectron. 79, 488–494.
Zhuang, J., Lai, W., Chen, G., Tang, D., 2014. Chem. Commun. 50, 2935–2938.